Negative Capacitance in InGaN/GaN Based LEDs from metal-semiconductor interfaces

Yuchen Li[1], Zhizhong Chen[1,2,3,*], Chuhan Deng[1], Boyan Dong[1], Daqi Wang[1], Zuojian Pan[1], Haodong Zhang[1], Jingxin Nie[1], Weihua Chen[1], Fei Jiao[1,4], Xiangning Kang[1], Qi Wang[2], Guoyi Zhang[1,2], Bo Shen[1,3], Wenji Liang[5]

1 State Key Laboratory for Artificial Microstructure and Mesoscopic Physics, School of Physics, Peking University, Beijing 100871, China

2 Dongguan Institute of Optoelectronics, Peking University, Dongguan, Guangdong 523808, China

3 Yangtze Delta Institute of Optoelectronics, Peking University, Nantong, Jiangsu 226000, China

4 State Key Laboratory of Nuclear Physics and Technology, School of Physics, Peking University, Beijing 100871, China

5 AET Displays Limited Co., Ltd, Dongguan, Guangdong, China

*E-mail: zzchen@pku.edu.cn

Abstract: To meet the demand for high-speed response in display applications, a more detailed study of the capacitive effects in LEDs is required. This work tested the capacitance of LEDs at different frequencies and proposed an effective capacitance model, which achieved a good fit to the frequency dispersion observed in the experimental results. Additionally, it was determined that the low-frequency 1/f capacitance originates from the metal-semiconductor interface.

Introduction

InGaN based light-emitting diodes (LEDs) have been widely used for display. When compared with liquid crystal displays, the high-speed response characteristics of LEDs are highly valued [6]. However, current LED displays are far from realizing the potential of active region photoelectric conversion in terms of response time. One of the key limitations comes from the capacitance effect in LEDs, or more specifically, the negative capacitance (NC) effect under forward bias.

Although NC in LEDs has been reported for quite some time, its frequency dispersion has not been fully investigated, and the cause of negative capacitance is still highly controversial. Shim et al. eliminated the negative capacitance by correcting the effects of the series resistance, thereby concluding that the negative capacitance is merely an artifact caused by the series resistance [3]. Feng et al. assumed that the carrier lifetime in the active region is much lower than in other regions, and thus derived the negative capacitance through the continuity equation [5]. Ershov et al. perform Fourier transform on the exponential decay form of transient current to obtain negative capacitance [4]. Their models all agree well with the experimental results they reported, but the common issue with these experimental results is that they were all C-V scans conducted only at one or a few specific frequencies. In order to further clarify the cause of negative capacitance, frequency scanning should be given the same attention as bias scanning [7].

Experimental methods

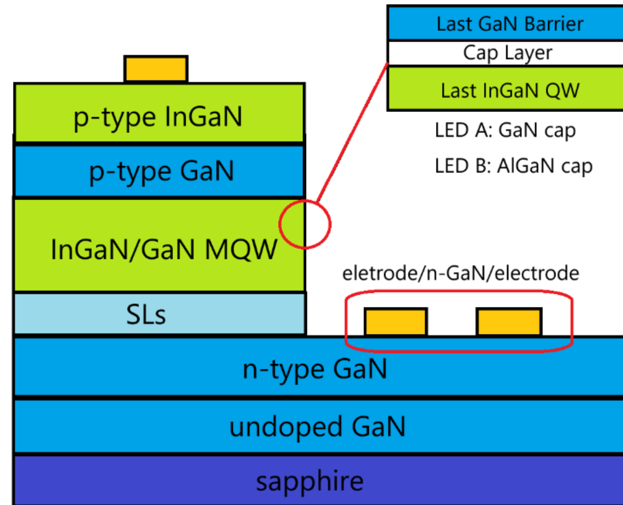

Figure 1: schematic diagram of the LED sample structure

As shown in Figure 1, LED samples were grown on 2-inch sapphire substrates in a MOCVD system. After substrate clean in H_2 at 1050°C, a GaN buffer layer was grown, followed by undoped GaN and n-GaN layers. The active region consists of 8 periods of SLs and 6 QWs. The growth time of all cap layers is 90s, under 90 mL/min TEGa flow at 830°C. Only when growing the last cap layer of LED B, a 50mL/min TMAl flow was introduced. Afterwards, p-layers containing LTp-GaN, p-GaN and p-InGaN were grown successively.

Capacitance measurements of LEDs have been conducted under different DC biases and different frequencies. The measurements are performed at room temperature (293K) using an Agilent4294A impedance analyzer.

The settings for the Agilent4294A impedance analyzer are as follows: the measurement parameter is selected as $C_p - g$ mode; the scanning parameter is selected as frequency; the AC amplitude is set to 30mV; the bandwidth is set to the maximum level of 5.The $C_p - g$ mode collects the current response of the LED under the joint drive of DC bias and AC voltage signal, and extracts the current response signal with the same frequency as the AC signal from the current response. This signal is decomposed into two parts: one part with the same phase as the AC drive signal and the other part with a phase difference of $\pi/2$. The part with the same phase is considered to be contributed by the conductance g, and the part with a phase difference of $\pi/2$ is considered to be contributed by the capacitance C_p. The current response of the LED is equivalent to the current response of a simple parallel system of capacitance C_p and conductance g.

Results and discussion

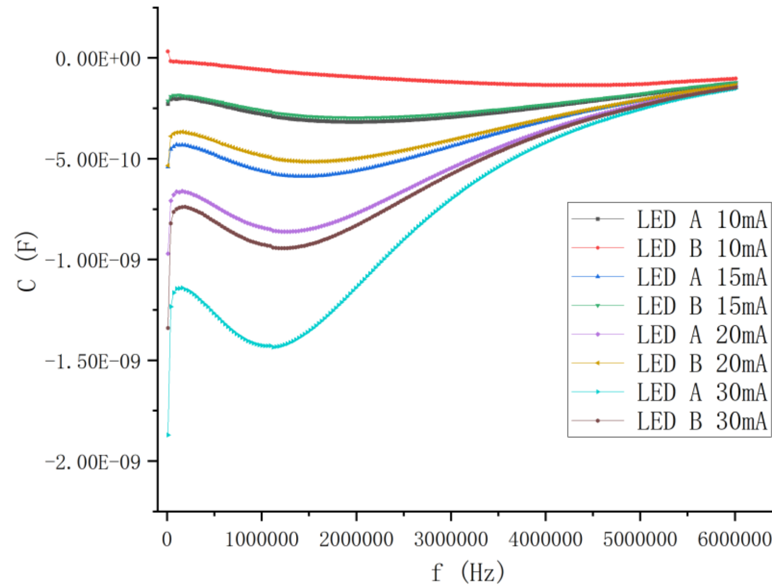

Figure 2: frequency dispersion of LED capacitance

Measured forward capacitance-frequency scan is shown in Figure. Both LED A and B show obvious negative capacitance phenomenon under forward bias. When same level of injection current applied, negative capacitance of AlGaN capped LED B is weaker compared to GaN capped A. (In Figure, the negative capacitance of LED A under 10mA injection happens to be nearly identical to LED B under 15mA)

Based on the behavior of the C-f curve, the frequency dispersion of negative capacitance can be roughly divided into three segments from high to low frequency. The first segment (>5MHz) shows minimal variation in negative capacitance with changes in current injection levels, and the impact of cap layer composition changes on negative capacitance is also insignificant. The second segment (~1MHz) exhibits more noticeable changes in negative capacitance with variations in current injection levels and cap layer composition. The third segment (<0.1MHz) distinctly differs from the second segment, displaying a unified low-frequency limit divergence trend, often referred to as 1/f negative capacitance in previous reports [4][8].

From such complex frequency dispersion, it can be inferred that negative capacitance may be contributed by multiple distinct mechanisms, each with its own frequency dispersion characteristics, leading to different dominant mechanisms at different frequencies. However, even when considering the results reported by Feng et al. and Ershov et al., the frequency dispersion cannot be fully explained. There are two main issues: First, the negative capacitance derived from both models tends to a constant value at the low-frequency limit [4][5], thus lacking the explanatory power for the 1/f negative capacitance observed at <0.1MHz. Second, both models provide limited information on the structural location of the physical processes, making it difficult to provide verification methods for adjusting capacitance by altering device structures.

While investigating the 1/f negative capacitance effect in the <0.1MHz range, it was unexpectedly found that the first batch of samples, which had suffered electrode damage due to excessively high annealing temperatures, exhibited significant changes in low-frequency capacitance. Consequently, the interface

between the electrode and the semiconductor has garnered attention.

The negative capacitance at the metal-semiconductor interface was reported as early as 1990 by Wu et al [1]. Due to the trust in "Ohmic contact," this effect seems to have not received sufficient attention in GaN-based devices. Wu et al. provided the following analysis of the capacitance at this interface:

According to charge conservation, the increment of interface state's occupancy probability $dF(t)/dt$ must equal the net electrons that enter the trap [1][2]:

$$\frac{dF(t)}{dt} = c_n[1 - F(t)]n_s(t) - e_nF(t) - c_pF(t)p_s(t) + e_p[1 - F(t)] - \frac{F(t) - F_m}{\tau_m} - \frac{a_n}{4}F(t)n_s(t) \quad (1)$$

where c_n (c_p) and e_n (e_p) are the electron (hole) capture coefficient and the electron (hole) emission constant; $n_s(t)$ and $p_s(t)$ are the free electron and hole densities at the semiconductor surface at time t; and F_m and τ_m denote the Fermi function in the metal and the metal-interface relaxation time, respectively.

Electrons that surmount the Schottky barrier under forward bias do fill up the empty states at the interface, but because they possess excess energy, when colliding with the electrons trapped at the interface states they could also knock electrons out of the traps, provided that the binding energy of these traps is smaller than the Schottky barrier energy. To describe this process, they modified the Shockley-Read model by adding an impact-loss term $-a_nF(t)n_s(t)/4$ into the expression of $dF(t)/dt$, which is proportional to the incident current density.

$F(t)$ can be expressed as the sum of a dc and an ac part:

$$F(t) = f + \delta f(t) \quad (2)$$

where f is the steady-state occupancy established by the de bias, and δf is the time variation caused by the ac signal. neglect the hole contribution (i.e., c_p= 0). Then using the principle of detailed balance, f and δf were derived:

$$f = F_s\frac{c_nn_{s0} + F_m/\tau_m}{(c_n + a_n/4)n_{s0} + F_s/\tau_m} \quad (3.1)$$

$$\delta f = \frac{\left[c_n(1 - f) - \frac{a_n}{4}f\right]\delta n_s}{(c_n + a_n/4)n_{s0} + \frac{1}{\tau_m} + j\omega} \quad (3.2)$$

Quantitative analysis of the capacitance curve is based on a two-energy level simplified model, where level 1 is located 0.25 e V above E_f^m and level 2 is assumed to be 0.1 eV below E_f^m. Then δf of both levels can be derived as:

$$\delta f_1 = \frac{c_n\delta n_s}{\tau_1\left[\left(c_n + \frac{a_n}{4}\right)n_{s0} + \frac{1}{\tau_1}\right]\left[\left(c_n + \frac{a_n}{4}\right)n_{s0} + \frac{1}{\tau_1} + j\omega\right]} \quad (4.1)$$

$$\delta f_2 = -\frac{a_n\delta n_s}{4\tau_2\left[\left(c_n + \frac{a_n}{4}\right)n_{s0} + \frac{1}{\tau_2}\right]\left[\left(c_n + \frac{a_n}{4}\right)n_{s0} + \frac{1}{\tau_2} + j\omega\right]} \quad (4.2)$$

The electron capture coefficient may be expressed ill terms of the electron capture cross section and the mean thermal velocity, i.e., $c_n = \sigma_n\bar{v}$. This leads to:

$$c_nn_{s0} = \sigma_n\bar{v}n_{s0} = 4\sigma_nJ/q \quad (5.1)$$

$$c_n \delta n_s = \sigma_n \bar{v} \delta n_s = 4\sigma_n \delta j/q \tag{5.2}$$

where J and δj are current densities in dc and ac, respectively. The factor of 4 comes from the consideration that $J = q\bar{v}n_{s0}/4$. Unlike n_{s0} and δn_s, the current densities J and δj can be obtained directly from the J-Vand the G-V measure ments; therefore, they are more accurate. Substituting Eq.5 into Eq.4, we end up with the expression:

$$\delta f_1 = \frac{4\sigma_n \delta j/q}{\tau_1 \left[(4\sigma_n + \sigma_i)J/q + \frac{1}{\tau_1}\right]\left[(4\sigma_n + \sigma_i)J/q + \frac{1}{\tau_1} + j\omega\right]} \tag{6.1}$$

$$\delta f_2 = -\frac{\sigma_i \delta j/q}{\tau_2 \left[(4\sigma_n + \sigma_i)J/q + \frac{1}{\tau_2}\right]\left[(4\sigma_n + \sigma_i)J/q + \frac{1}{\tau_2} + j\omega\right]} \tag{6.2}$$

where σ_i is the impact-loss cross section. The capacitive effect is contributed by the imaginary part of δf, leading to the derivation of:

$$C_1 = -\frac{q^2 I N_{s1}}{\omega(kT + qIR_s)C_i \Delta V} Im(\delta f_1) = \frac{\frac{qIN_{s1}4\sigma_n}{(kT + qIR_s)C_i}\frac{\delta j}{\Delta V}}{\tau_1 \left[(4\sigma_n + \sigma_i)J/q + \frac{1}{\tau_1}\right]\left\{\left[(4\sigma_n + \sigma_i)J/q + \frac{1}{\tau_1}\right]^2 + \omega^2\right\}} \tag{7.1}$$

$$C_2 = -\frac{q^2 I N_{s2}}{\omega(kT + qIR_s)C_i \Delta V} Im(\delta f_2) = -\frac{\frac{qIN_{s2}\sigma_i}{(kT + qIR_s)C_i}\frac{\delta j}{\Delta V}}{\tau_2 \left[(4\sigma_n + \sigma_i)J/q + \frac{1}{\tau_2}\right]\left\{\left[(4\sigma_n + \sigma_i)J/q + \frac{1}{\tau_2}\right]^2 + \omega^2\right\}} \tag{7.2}$$

where $C_i = \epsilon_i/\delta$ is called the interface specific capacitance, described by interface thickness, δ, and the permittivity, ϵ_i.

From Eq.7, two points can be observed: first, the source of the interface negative capacitance is primarily the trap states below E_f^m at the interface; second, the frequency dispersion of the interface negative capacitance is consistent with the results reported by Ershov et al [4]. This could potentially help elucidate the corresponding structural origins in the work of Ershov et al. Using the parameter values employed by Wu et al. in their simulations [1], similar C-V characteristics can be obtained.

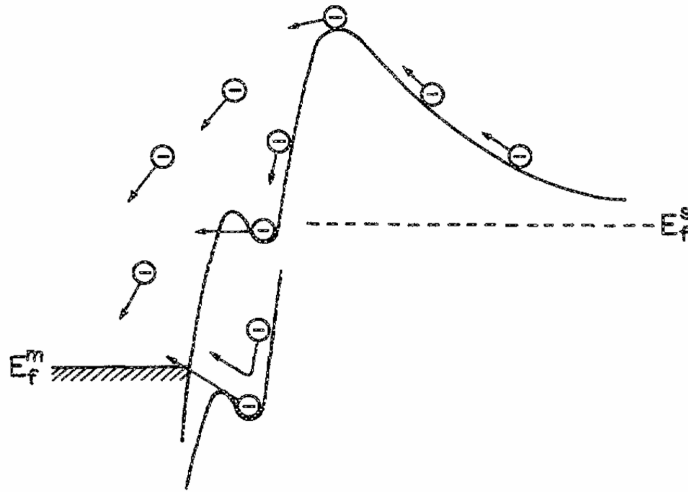

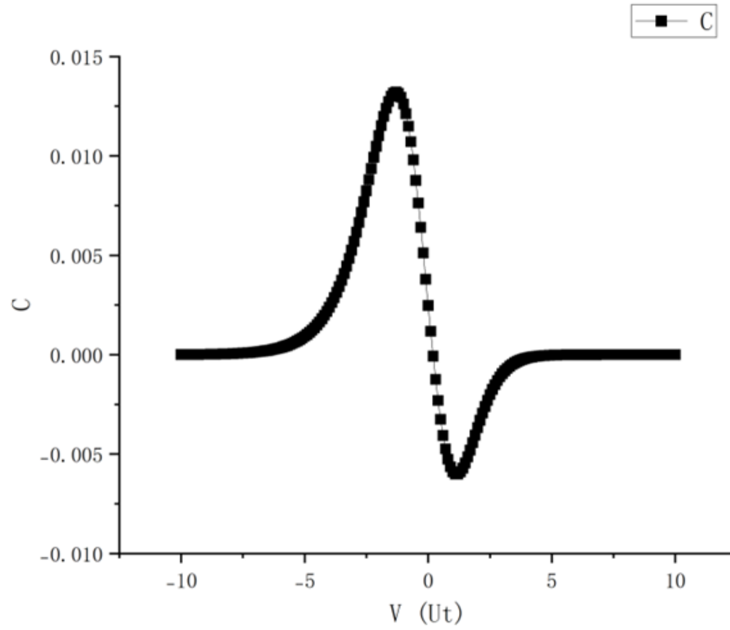

Figure 3: (a) a “waterfall” model by Xu et al. , showing the electron capture and reemission process, as well as the electron impact ionization at the interrace. [1] (b)C-V schematic diagram of the interface capacitance (Using an approximate I-V exponential relationship here, without series resistance).

To eliminate the influence of other structures in the LEDs and verify the aforementioned theoretical model, an electrode/n-GaN/electrode structure was conveniently prepared at the alignment mark during the LED chip fabrication process. Additionally, Huangshu Zhang provided electrode/n-AlN/electrode samples. C-V-f measurement results of these samples are shown in Fig 4.

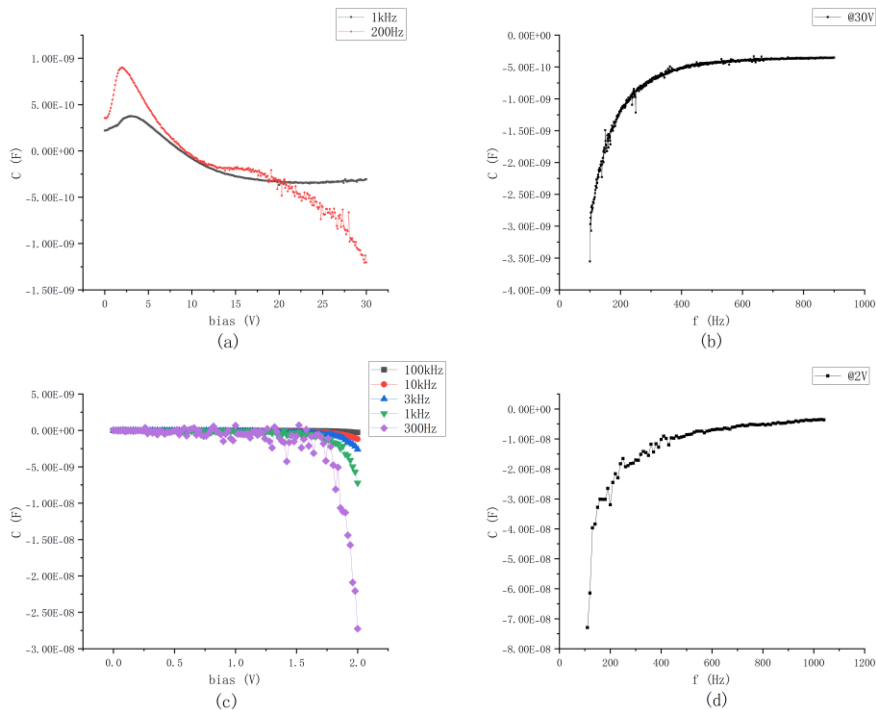

Figure 4: C-V-f test results of the metal/semiconductor/metal structure sample:

(a) C-V characteristics of the n-AlN sample, (b) 1/f capacitance in n-AlN sample,

(c) C-V characteristics of the n-GaN sample, (d) 1/f capacitance in n-GaN sample.

From Figure 4(a), it is observed that the C-V behavior of the AlN sample at 1kHz closely matches the results of Xu et al., particularly the trend of negative capacitance saturation and rollback with increasing bias. However, at 200Hz, this saturation trend disappears. Combined with the C-f scan results in Figure 4(b), it can be inferred that this change is due to the emergence and dominance of 1/f negative capacitance. As shown in Figure 4(d), the GaN sample also exhibits dominant 1/f negative capacitance at low frequencies. However, contrary to expectations, no trend of negative capacitance saturation and rollback was observed in the GaN sample, shown in Figure 4(c). Even at frequencies as high as 6MHz, the capacitance continuously changes monotonically when applied high bias.

Although the aforementioned results indicate that the model proposed by Wu et al. can only partially explain the capacitance at the III-V semiconductor and metal interface, and difficulties remain in explaining the 1/f capacitance; through capacitance testing of the metal/semiconductor/metal structure, we have sufficient reason to make the following judgment: the previously reported 1/f negative capacitance does not originate from the electro-optical conversion process in the quantum wells of the active region, but rather from the interface between the metal electrode and the semiconductor. Particularly, by comparing Figures 2 and 4(d), in samples with only interface structures and similar area, the 1/f negative capacitance appears at low frequencies, and its magnitude is similar to that of the LED samples. In previous reports on 1/f negative capacitance, it was often vaguely attributed to carrier recombination. Therefore, pinpointing the location of the 1/f negative capacitance to the metal-semiconductor interface is a significant advancement.

Now we can return to the frequency dispersion of the LED capacitance in Figure 2 and attempt to reconstruct the composition of the capacitance: First, in the lowest frequency band, the 1/f negative capacitance dominated by the electrode-semiconductor interface is observed. As the frequency increases, the negative capacitance most relevant to the injection state and structure of the active region dominates around 1MHz. Although Wu et al.'s model cannot be directly applied to analyze the semiconductor heterojunction interface here, it can provide a relatively reasonable image of frequency dispersion: that is, the interface states above the Fermi level contribute positive capacitance, while the states below the Fermi level contribute negative capacitance. Finally, at frequencies above 5MHz, the capacitance relative to the changes in the injection state and structure of the active region is already much smaller compared to around 1MHz, and the frequency dispersion is similar to Feng et al.'s model [5]. The overall frequency dispersion of the LED capacitance can be expressed in the following form:

$$C(\omega) = -\frac{C_1}{\omega\tau_1} + \frac{C_2}{1+(\omega\tau_2)^2} - \frac{C_3}{1+(\omega\tau_3)^2} + C_4\frac{\sqrt{\sqrt{1+(\omega\tau_4)^2}-1}}{\omega\tau_4} \tag{8}$$

where the last term comes from $Im(\sqrt{1+j\omega\tau_4})$ [5]. Using Eq.8 to fit the experimental results in Figure.2, the frequency dispersion is successfully reproduced, as shown in Figure.5.

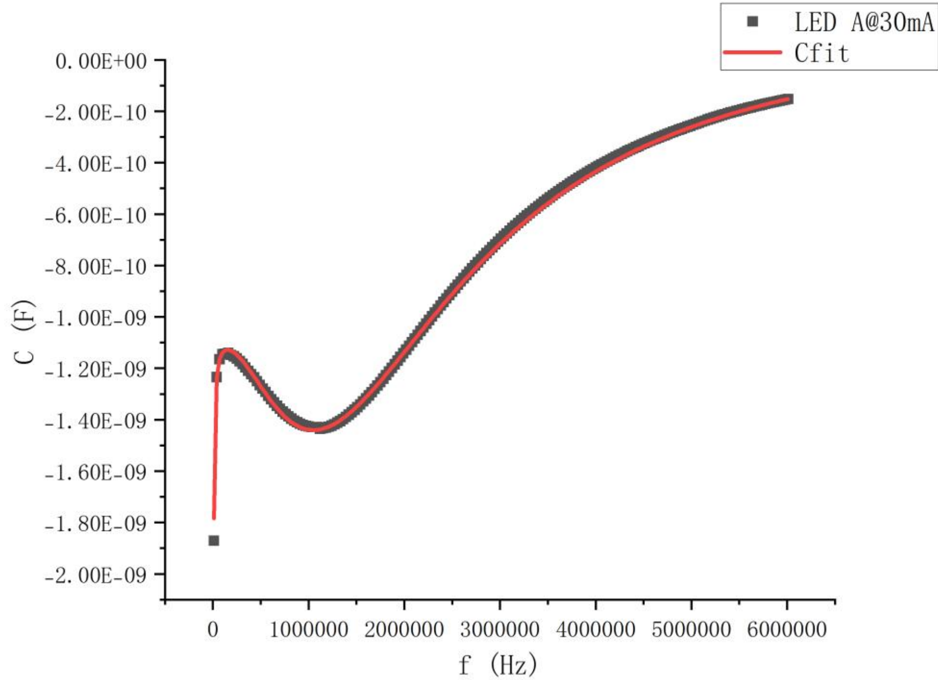

Figure 5: fitting results of frequency dispersion by Eq.8

Conclusion

Overall, the capacitance of LEDs can be attributed to three mechanisms: first, the 1/f capacitive effect at the interface; second, the impact loss of occupied interface states under electron injection; and third, the diffusion capacitance modified by continuity equation. This model can adequately explain the variation of capacitance with frequency. The next step will be to seek a theoretical explanation for the 1/f capacitance at the interface.

Acknowledgment

This work was supported by National Key Research and Development Program (2023YFB4604400); National Natural Science Foundation of China (62174004, 61927806); and Guangdong Basic and Applied Basic Research Foundation (2020B1515120020).

References

1. Wu, X., Yang, E. S., & Evans, H. L. (1990). Negative capacitance at metal-semiconductor interfaces. Journal of applied physics, 68(6), 2845–2848.

2. Wu, X., & Yang, E. S. (1989). Interface capacitance in metal-semiconductor junctions. Journal of applied physics, 65(9), 3560–3567.

3. Han, D.-P., Kim, Y.-J., Shim, J.-I., & Shin, D.-S. (2016). Forward-Capacitance Measurement on Wide-Bandgap Light-Emitting Diodes. IEEE photonics technology letters, 28(21), 2407–2410.

4. Ershov, M., Liu, H. C., Li, L., Buchanan, M., Wasilewski, Z. R., & Jonscher, A. K. (1998). Negative capacitance effect in semiconductor devices. IEEE transactions on electron devices, 45(10), 2196–2206.

5. Feng, L. F., Li, Y., Zhu, C. Y., Cong, H. X., & Wang, C. D. (2010). Negative Terminal Capacitance of Light Emitting Diodes at Alternating Current (AC) Biases. IEEE journal of quantum electronics, 46(7), 1072–1075.

6. Pan, Z. J., Chen, Z. Z., Jiao, F., Zhan, J. L., Chen, Y. Y., Chen, Y. F., Nie, J. X., Zhao, T. Y., Deng, C. H., Kang, X. N., Li, S. F., Wang, Q., Zhang, G. Y., & Shen, B. (2020). A review of key technologies for epitaxy and chip process of micro light-emitting diodes in display application. Wuli xuebao, 69(19), 64–87.

7. Gong, Y., Zhang, L., Lin, P., Yuan, Z., Peng, L.-M., & Kang, J. (2024). P-140: The Miniaturization of InGaN/GaN Micro-LEDs for Micro-Displays – Size Effects, Frequency Dispersion and Compact Modeling. SID International Symposium Digest of technical papers, 55(1), 1928–1931.

8. Sato, S., Takada, M., Kawate, D., Takata, M., & Naito, H. (2019). Negative capacitance of bilayer organic light-emitting diodes-its correlation with current efficiency and device lifetime. Japanese Journal of Applied Physics, 58(SF), SFFA01.